AIP | Review of Scientific Instruments

A portable molecular beam epitaxy system for in situ x-ray investigations at synchrotron beamlines

T. Slobodskyy, P. Schroth, D. Grigoriev, A. A. Minkevich, D. Z. Hu, D. M. Schaadt, and T. Baumbach

Citation: Review of Scientific Instruments **83**, 105112 (2012); doi: 10.1063/1.4759495
View online: http://dx.doi.org/10.1063/1.4759495
View Table of Contents: http://scitation.aip.org/content/aip/journal/rsi/83/10?ver=pdfcov
Published by the AIP Publishing

A portable molecular beam epitaxy system for *in situ* x-ray investigations at synchrotron beamlines

T. Slobodskyy,[1,2,a)] P. Schroth,[1] D. Grigoriev,[1] A. A. Minkevich,[1] D. Z. Hu,[3,4] D. M. Schaadt,[3,4] and T. Baumbach[1]

[1]*Institute for Synchrotron Radiation, Karlsruhe Institute of Technology - 76344 Eggenstein-Leopoldshafen, Germany*
[2]*Institut für Angewandte Physik und Zentrum für Mikrostrukturforschung, Jungiusstraße 11, D-20355 Hamburg, Germany*
[3]*Institute for Applied Physics/DFG-Center for Functional Nanostructures, Karlsruhe Institute of Technology (KIT), Karlsruhe, Germany*
[4]*Institute for Energy Research and Physical Technologies, Technical University Clausthal, Am Stollen 19B, 38640 Goslar, Germany*

(Received 17 July 2012; accepted 3 October 2012; published online 19 October 2012)

A portable synchrotron molecular beam epitaxy (MBE) system is designed and applied for *in situ* investigations. The growth chamber is equipped with all the standard MBE components such as effusion cells with shutters, main shutter, cooling shroud, manipulator, reflection high energy electron diffraction setup, and pressure gauges. The characteristic feature of the system is the beryllium windows which are used for *in situ* x-ray measurements. An UHV sample transfer case allows *in vacuo* transfer of samples prepared elsewhere. We describe the system design and demonstrate its performance by investigating the annealing process of buried InGaAs self-organized quantum dots. © *2012 American Institute of Physics*. [http://dx.doi.org/10.1063/1.4759495]

I. INTRODUCTION

The molecular beam epitaxy (MBE) is a versatile technique allowing precise control over the deposition environment in a wide range of growth conditions.[1] It is often used for deposition of self-organized nanostructures on semiconductor surfaces.[2] Improvement of the properties of the nanostructures beyond current state of the art requires understanding of dynamical processes during self-organization. Strain induced interaction between the nano-objects[3] as well as change in the strain state of the nanostructures during deposition and annealing[4] are of specific interest for the scientific community.

The strain state of the nanostructures can be accessed using x-ray diffraction.[5] Laboratory x-ray diffractometers are routinely used for strain investigation. The diffractometers, however, hardly permit integration of such a demanding equipment as a growth chamber for MBE into the measurement setup. Beside this, the intensity of the x-ray beam produced using laboratory setup is not sufficient to characterize dynamical processes at nanoscale with sufficient time resolution.

High brilliance synchrotron radiation provides a way to overcome these difficulties.[6] The high brilliance of the x-ray beam allows for fast scan repetition and highly parallel beam permits reasonable size of the deposition equipment. Therefore we decided to use synchrotron radiation for investigation of dynamical processes during MBE deposition.

In the past there have been several approaches to combine UHV equipment and MBE systems with synchrotron diffractometers.[7–16] In principle, these concepts can be separated to two general philosophies.

The first approach is to use a large stationary UHV system in which a diffractometer is integrated. This is usually advantageous in terms of vacuum quality and growth conditions, because the overall weight of the MBE components is not limited by additional constraints such as mobility of the system. This holds as well for the vacuum system, and supplementary surface analysis equipment. In this case, however, a complete beamline has to be dedicated to this single purpose.

The second approach is to utilize a small lightweight UHV chamber that is installed at a suitable diffractometer at a synchrotron beamline on demand. The latter approach often lacks adequate control over the growth parameters and scanning motions of the diffractometer. Yet, it gives versatile possibilities in choosing the appropriate beamline suitable for the particular x-ray experiment. We chose the latter philosophy in order, to have a standalone MBE system which, nevertheless is portable and suitable to be mounted on a diffractometer at a synchrotron beamline of our choice.

In this paper, we describe a portable UHV system which can be used at various beamlines but without compromising on quality of epitaxial nanostructures. The system is developed for *in situ* investigations of growth and evolution of epitaxial semiconductor nanostructures.

II. SYSTEM LAYOUT AND TECHNICAL DESIGN

It was our aim to design a portable MBE system which should be able to transport and process samples grown at the MBE clusters of our collaboration partners under UHV conditions. In addition growth of nanostructures should be possible within this chamber when it is mounted on the diffractometer and the x-ray experiment is running. The system should

[a)]Taras.Slobodskyy@physik.uni-hamburg.de.

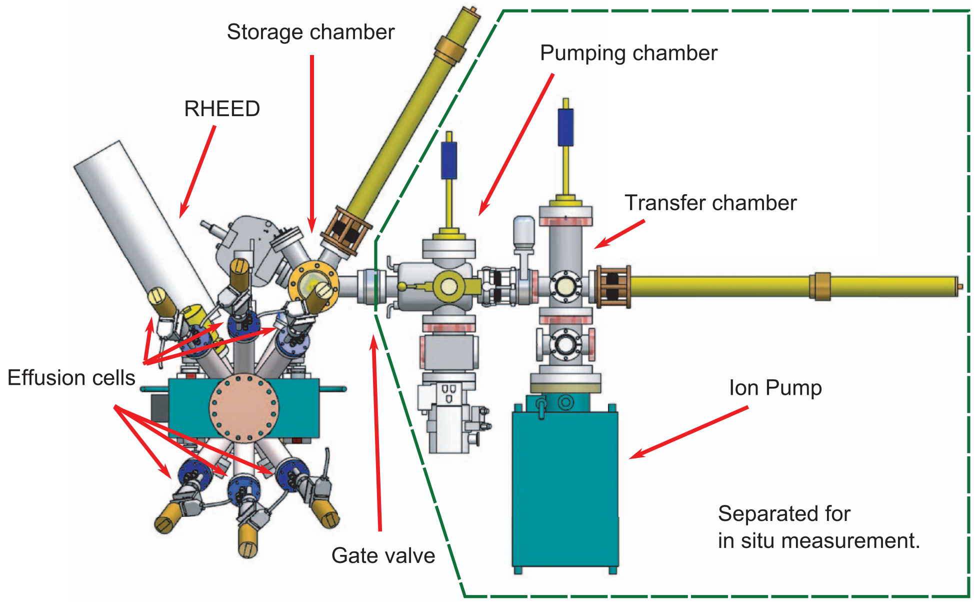

FIG. 1. Scheme of the portable MBE system. The green box indicates the transfer case which is separated during x-ray experiments.

offer a possibility for x-rays to enter, hit the sample, and leave the chamber in a widest angular range possible, to afford x-ray investigations. Let us now discuss how these aims were realized.

The portable MBE system comprises three main parts: a unit for sample UHV transfer and loading called transfer case (TC), a unit for sample storage called storage chamber (SC), and a chamber for MBE growth called growth chamber (GC), featuring two beryllium windows for the x-rays as it depicted in the Fig. 1. To make this system as versatile and mobile as possible, these three parts are located on a steel frame supported by wheels.

The SC and GC can be decoupled from the TC and relocated from the frame onto the diffractometer for x-ray measurements. To maintain the vacuum during each step of the experiment, each separate chamber is individually pumped.

Despite the fact, that specialized equipment and parts could yield a considerable decrease in the weight of the UHV system, we resort to standard CF components where it is possible. Therefore, the UHV system comprising of GC, SC, and TC has a total weight of 350 kg. Standard components, however, reduce delays in the case of component failure and decrease operational costs. Consider that the combined GC and SC weight is about 155 kg only.

Experimental layouts have been realized at the NANO beamline at ANKA—the synchrotron facility at the Karlsruhe Institute of Technology (KIT) and at the surface diffraction beamline ID03 at the European Synchrotron Radiation Facility (ESRF), where the first *in situ* measurements have been performed.

A. Growth chamber

The GC is used for MBE-growth. The inner diameter of the GC is 250 mm. A cooling shroud is installed into a CF150 flange, and a CF100 flange is used for the ion pump which is equipped with a titanium sublimator. Two CF100 flanges are dedicated to standard 90 mm beryllium x-ray windows. CF40 ports for sample transfer, reflection high energy electron diffraction (RHEED) gun and RHEED screen as well as two view port flanges are present. Six CF40 flanges are pointing to the sample surface and can be used to install effusion cells.

In the present configuration, three of the effusion cells are used for growth of InGaAs compounds, pointing at the sample surface normal at an angle of 30°. The effusion cells for indium and gallium are high temperature dual-filament cells whose crucibles and tips can be separately heated. The effusion cell for arsenic is a low temperature cell with one heating zone. The cells are equipped with fast shutters in front of the cell's orifices.

The GC is equipped with a main shutter which can be positioned in front of the sample to protect the surface during the effusion cells adjustments. The precise positioning of the shutter can also be used for low resolution shadow epitaxy when it is required.[17]

A manipulator is responsible for sample positioning featuring translation and endless-rotation is motorized by brushless DC servo-motors "Faulhaber." A pneumatically actuated stabilization stamp can fix the sample position during x-ray measurements. Using the manipulator, the sample can be positioned such that RHEED and x-ray measurements can be performed at the same time. In this configuration the sample is located in the center between the beryllium window ports. Tungsten heating wires provide sample heating. The sample heater supports heating up to T = 900 °C. The temperature at the sample is measured by a thermocouple located in the substrate heater near to the substrate.

The sample is mounted such that its surface normal points in horizontal direction. This is necessary to avoid a decrease of the scattered intensity due to polarization effects for high scattering angles in grazing incidence diffraction (GID) geometry, keeping in mind, that synchrotron radiation is

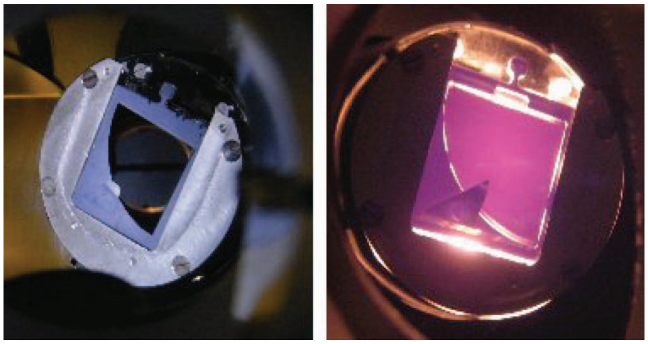

FIG. 2. Left: View of a sample mounted on the manipulator. Right: Heating uniformity of the sample at high temperature.

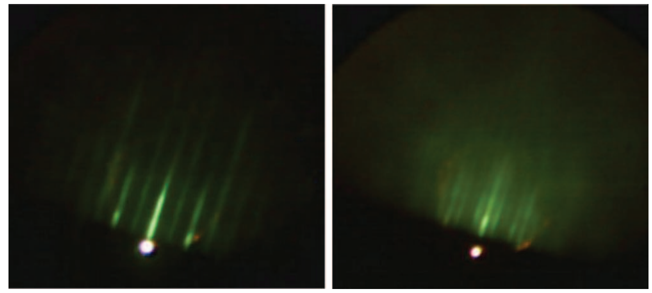

FIG. 3. (2 × 4) RHEED reconstruction of a GaAs surface after oxide desorption observed during an *in situ* experiment.

polarized in the horizontal plane. We designed a special sample-holder to keep the sample in its vertical position, not blocking RHEED or x-ray beams.

The standard samples used in our system have the size of a quarter of a 2" wafer. The samples are fixed to the sample holder by a clamp. This reduces the contact area and therefore minimizes strains induced in the wafer. A homogeneous temperature distribution on the sample is achieved by using a large opening in the sample holder. The sample size allows complete projection of the incoming beam in the grazing incidence geometry. Thus avoiding the unfavorable edge effects of the scattered and reflected beams.[10] Figure 2 shows a view of a sample mounted on the manipulator. The sample is seen at different temperatures and from different view ports.

Three view ports are installed to visually check the sample position for transfer. Additionally, the view ports are used for a LASER pre-alignment of the sample surface during x-ray measurements. The two beryllium-windows, located on the opposite sides of the deposition chamber (see Fig. 4), allow *in situ* x-ray measurements. Motorized shutters in front of the beryllium-windows prevent the contamination of the beryllium-windows during growth when no x-ray experiments are performed. The same shutters can be used as in-vacuum x-ray beam stop to decrease the effect of parasitic scattering on the exit Be-windows when it is needed.

A cold-cathode pressure gauge "Pfeiffer" provides information about the vacuum conditions in each of the chambers. A 100 l/s ion pump "Gamma Vacuum" combined with a titanium sublimation pump achieve vacuum conditions with a base pressure in the lower 10^{-11} mbar range. The cells and the manipulator are water-cooled. Chilled water or liquid nitrogen can be supplied to the cryoshroud of the GC to improve vacuum conditions even further.

A 30 keV RHEED gun "SPECS" is operated for monitoring the growth process. The RHEED pattern is projected to an opposing fluorescence screen on a CF40 flange (pink line Fig. 4, left). Besides RHEED is an effective tool to investigate the surface quality and growth speed, it is commonly used to monitor the growth of nanostructures, especially to determine the 2D-3D transition during quantum dot growth, for example. Utilizing the motorized manipulator for sample rotation various surface reconstructions can be investigated. Two RHEED patterns of a (2 × 4) GaAs surface are shown on the Fig. 3.

B. Storage chamber

The storage chamber (SC) is directly connected to the GC. It is equipped with a magnetically operated storage cassette. This cassette can hold up to four samples. Using the transfer rod connected to the SC the samples are transferred into the GC and placed onto the manipulator for growth and x-ray investigation. During growth, the two chambers are isolated via a gate valve and the SC is pumped separately by a 10 s ion pump "Gamma Vacuum."

C. Transfer case

This part of the portable MBE system is used for UHV sample transfer to and from other MBE clusters and beamlines, like the III/V MBE cluster at the Center for Functional Nanostructures (CFN) at KIT to the dedicated synchrotron beamlines at ANKA or ESRF, respectively.

As well as the GC and SC, the TC consists of two individually pumped UHV parts which can be separated via a gate valve. The pumping chamber is used as a load-lock for inserting samples. It can be vented with dry nitrogen. Vacuum is achieved by a turbo molecular pump (TMP) "Pfeiffer" connected to a scroll pump. The pressure is measured by a cold-cathode wide range gauge "ATMION." An infra-red heating lamp can be used to degas the loaded samples.

After degassing in the pumping chamber, the samples can be transferred into the SC or into the second chamber of the TC where up to 10 samples can be stored in the storage cassette. The chamber holding the storage cassette can be isolated from the pumping chamber by a CF40 gate valve, and is pumped separately by a 150 l/s ion pump "Gamma Vacuum" and a TSP to achieve best possible vacuum during the sample transfer and storage. The pressure is monitored by a Bayard-Alpert hot cathode pressure gauge.

D. Integration and MBE control software

Due to hazardous radiation inside of the experimental hutch during synchrotron *in situ* experiments the MBE system should be fully automated and remotely controlled. All of the MBE system components should work simultaneously and synchronously. They also should interact with the beamline control software. Consequently already available standard solutions could not be easily adapted for our needs.

For the control purpose we have written a home made multithreading MBE control software, which is scriptable, object oriented, and cross-platform. Bidirectional communication with SPEC and Tango is already realized in the software. Extension to other interfaces should not be difficult through python written drivers.

The effusion cells shutters, main shutter, beryllium window shutters, manipulator translation, and rotation are controlled using precise position sensitive servo motors. This allows for precise adjustment of the experimental conditions without external intervention. The cells temperatures are controlled by digital controllers "Eurotherm". And pressure inside of all of the UHV components is monitored using cold cathode gauges as it is mentioned before.

The MBE control software is written in Python. Some of the advantages of this programming language are the easy syntax, cross platform nature and rich scientific libraries which facilitate application of this interpreted programming language in various areas of scientific and automation tasks. The graphical interface is realized using wxWidgets but can be easily transfered to Qt or GTK+.

The control software makes use of the internal python interpreter through Python execution calls. Functions specific for our automation tasks are predefined in the execution environment. The interpreter provides us with a complete, mature, and verified script execution environment. The Python syntax of the scripts makes it easy to learn to operate the software. The interpreter also takes care about the syntax, logic, threads, and interfaces.

The equipment is controlled using standard Ethernet topology through TCP/IP socket communication. For some control devices Ethernet to RS232 converters are used for interfacing. The control software is usually executed on a standard notebook computer without special adaptations. This makes the setup very flexible and failure prone, since the control computer can be rapidly replaced.

Multiple scripts can be executed, paused, and interrupted simultaneously. Execution environment of an individual script can be accessed from the command line.

During operation of the MBE software several threads are normally executed simultaneously performing such tasks as communication to the devices, recording of the growth and vacuum conditions, communication with beamline software, and execution of user growth scripts.

E. RHEED software

Reflection high energy electron diffraction is routinely used for growth monitoring. The CF40 RHEED view port of our growth chamber is located on the distance of 300 mm from the center of the substrate. This provides sufficient angular range for electron diffraction pattern observation at 24 keV. The electron gun provides sufficiently small focal spot compensating for degradation of angular resolution of the setup due to small sample-screen distance.

We use also a home made software for observation of RHEED patterns. The RHEED software can communicate with the MBE growth software. This allows us to synchronize sample rotation and growth stages with surface morphology observed through RHEED patterns. The data can be also streamed through the network to another computer for remote operation during *in situ* experiments.

The RHEED analysis software is written in python programming language and uses standard windows DirectShow video capture interface. In this manner various video-capture devices (e.g., a USB webcam) can be connected simultaneously and can be accessed on demand. The software was tested with few consumer webcams providing frame rates of up to 35 frames per second ($\approx$30 ms time resolution) and image resolutions of up to 1600 $\times$ 1200 pixels.

Flexible scripting allows the analysis software to be used for simultaneous pattern profiling. Currently implemented scripts include region of interest intensity monitoring for growth rate determination, linear profile evolution for lattice constant measurements, and frame recording for later analysis. The collected data are normally recorded to the hard drive in real time using common formats (e.g., ASCII, PNG, TIFF, and JPG).

Sample images of RHEED reconstructions collected using the software are shown in the Fig. 3.

III. X-RAY EXPERIMENT LAYOUT

Crucial for x-ray measurements are the Beryllium windows, fabricated by Brush Wellman, electrofusion products. The two Be-windows are mounted on CF100 standard flanges which allow for a vacuum in the lower 10^{-11} mBar range. The Beryllium foil used in the windows has a thickness of 300 μm.

Both windows are installed at opposing sites at the growth chamber, facing the manipulator (see Fig. 4). Thus, it is possible to apply surface sensitive x-ray diffraction methods like GID and grazing incidence small angle x-ray scattering (GISAXS) within an angular range of $\pm 18^\circ$ with respect to the incident beam (Green lines). Furthermore, optical reflectivity measurements can be applied to investigate the morphology of the grown layers. As it can be seen, the sample position is such that the surface normal points into horizontal direction.

For x-ray measurements, the GC together with SC are detached from the transfer case and mounted on the diffractometer at a suitable synchrotron beamline (see Fig. 4, right). Due to the 155 kg weight of the growth chamber a heavy-duty diffractometer (e.g., ID03 at ESRF or NANO at ANKA) is required.

If the diffractometer does not support heavy weight, e.g., $m_{GC} = 155$ kg, a weight-compensation device using a ceiling mounted crane in the experimental hutch can be employed to partially release weight-load from the diffractometer. This, however, should be used with care since it is difficult to balance the torque and the moments of inertia at the same time, especially while operating a multi-axis positioning system "Huber tower."

We used a special adaptor plate to mount the growth chamber on the diffractometer at ID03 for our first *in situ* experiment. This adaptor plate is used to incline the chamber with respect to the horizontal plane to an angle of 13°.

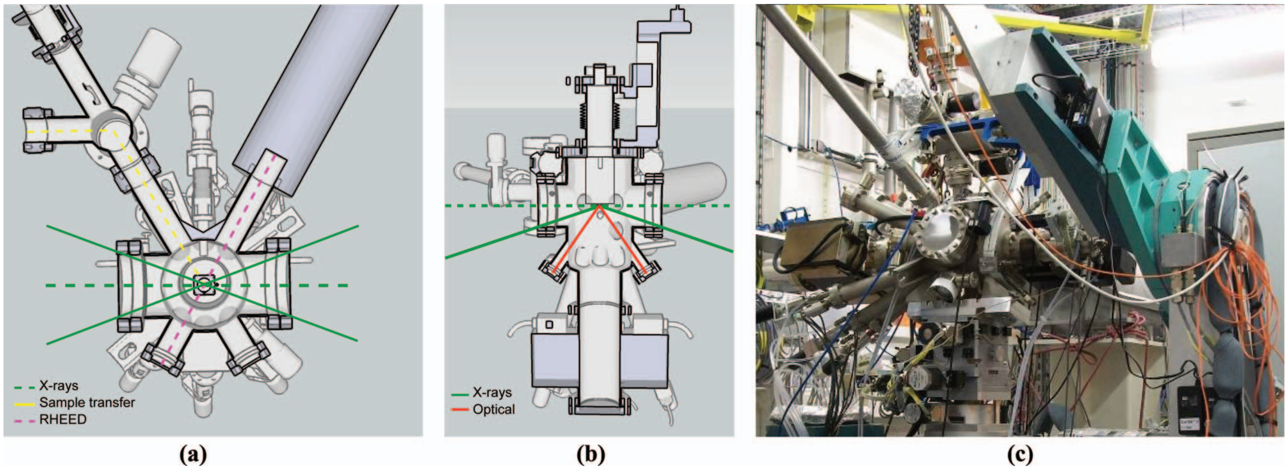

FIG. 4. (a) Vertical cut through growth chamber. The sample position is in the crossing points of the lines. Pink: RHEED, green: x-ray, and yellow: sample transfer. (b) Horizontal cut through growth chamber. Green: x-ray, orange: optical, and blue: material from effusion cells. (c) Growth chamber installed at ID03 vertical diffractometer, ESRF. Left: Effusion cells, ion pump and TSP. Center: Beryllium window pointing to the detector with flight tube. Right: Diffractometer detector arm.

Hence, the goniometer movement is closer to the [220] GaAs Bragg reflection and the accessible angular range 2θ is enlarged from 18° to 31°.

After mounting the chamber on the diffractometer the sample alignment is done using the x-ray beam. Once the proper measurements conditions are reached for one of the samples a laser pointer is installed so that the laser beam comes through one of the view windows and hits the sample. In this configuration the reflected laser beam is projected on one of the walls of the experimental hutch. The position of the reflected beam is labeled on the wall. This position is then used for all the following samples as a point of reference for alignment. This procedure speeds up the alignment procedure during *in situ* measurements.

Choosing the appropriate energy such that reflected and diffracted beam make an angle less than 31°, GID and GISAXS measurements can be performed simultaneously (see Fig. 5). In our case [220] GID reflex of InGaAs QDs could be reached using 13 keV photon energy. Detector frames during simultaneous GID and GISAXS measurements are shown below in Fig. 6.

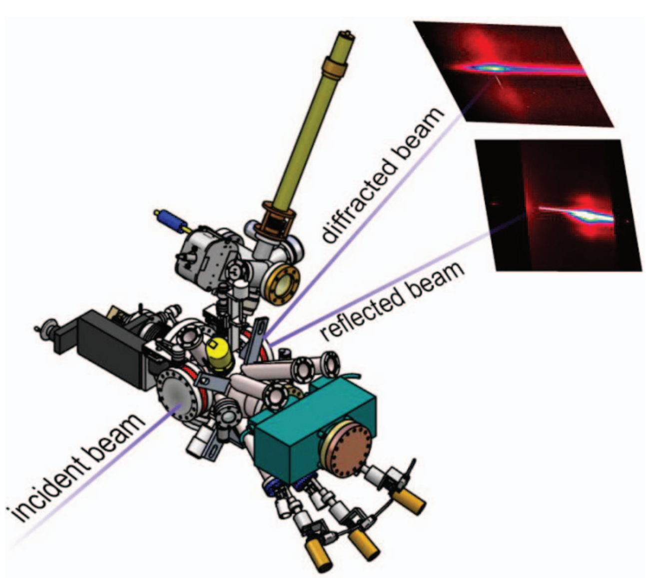

FIG. 5. Sketch of the GID and GISAXS measurement geometry.

IV. EXEMPLARY RESULTS AND DISCUSSION

In this section, we present exemplary experimental results received during *in situ* measurements in GID geometry during post-growth annealing, using the portable MBE system. We investigated a sample, grown at the CFN, featuring InAs QD overgrown by a 1.3 ML AlAs layer and 5 nm GaAs. The x-ray measurements were performed at the surface diffraction beamline ID03 at the ESRF.

The sample was transported in the TC to the ESRF under UHV conditions. Uninterrupted power supplies provided electricity for the pumping system during the transport. An UHV connection between SC and TC was established and the sample was inserted into the GC. The GC and SC itself were then mounted on the diffractometers "Huber tower," where a LASER sample alignment was done.

A Maxipix single chip CCD detector was used to measure the scattered intensities. The Maxipix gives an advantageous high time resolution, the integration time was 1 s per

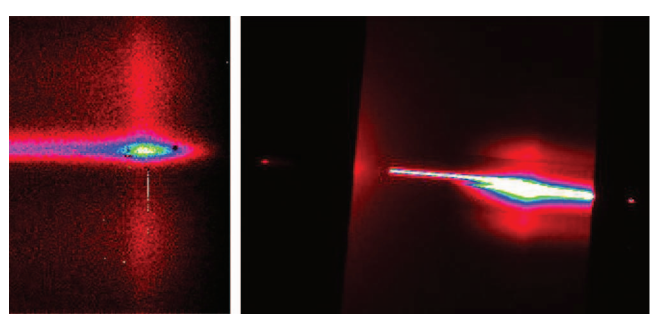

FIG. 6. Left: A single CCD image near to GaAs [220] GID reflex. Right: A frame in GISAXS geometry simultaneously recorded with a MarCCD detector.

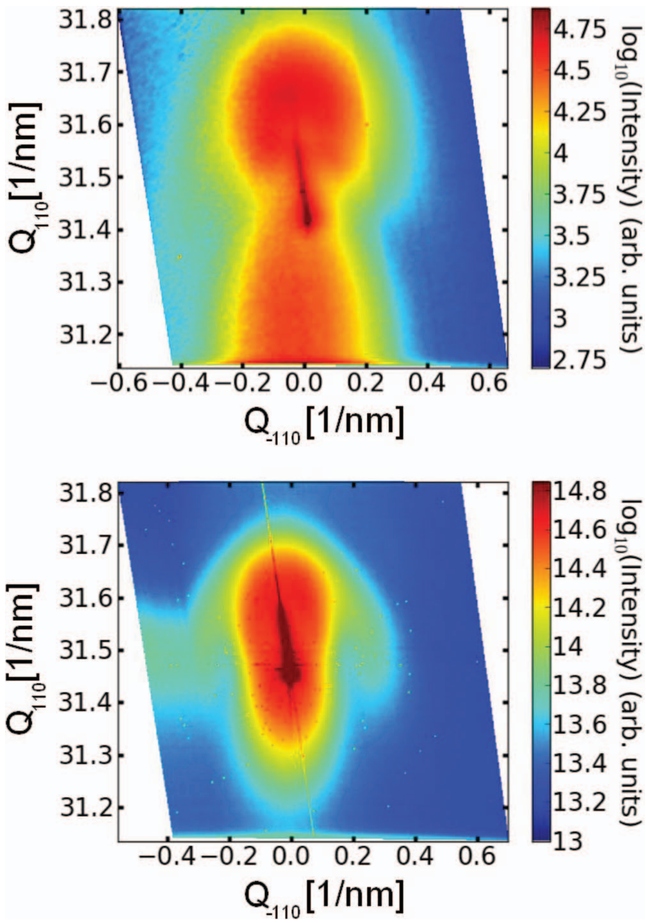

FIG. 7. Reciprocal space maps of the [220] GaAs bragg peak measured *in situ* using a photon energy of $E = 13$ keV at an incidence angle of $\alpha_i = 0.5°$. Top: before annealing. Bottom: after annealing (see text).

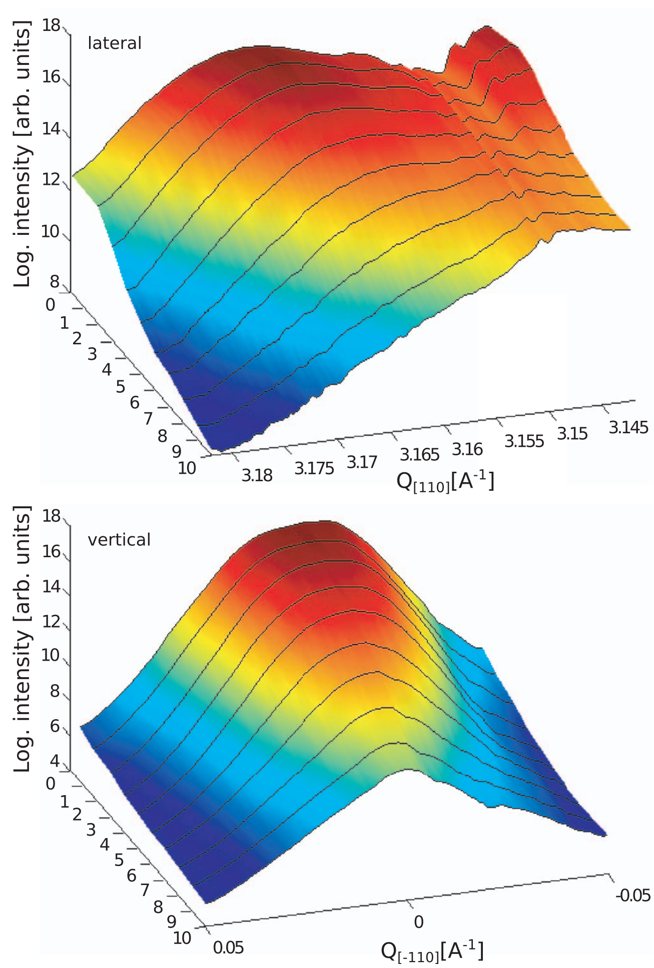

FIG. 8. Top: Time evolution of scattered signal intensity profiles in Q_{110} direction taken at $Q_{-110} = -0.0014$ 1/A. Bottom: Time evolution of profiles in Q_{-110} taken at around $Q_{110} = 3.1622$ 1/A. The profiles can be understood as lateral and vertical slices through Fig. 7. The numbers indicate evolution of the measured signal during the annealing process as described in text.

frame. Furthermore, a 2D detector enables us to measure a 3D volume of the reciprocal space. In GID configuration an additional information about the scattering component vertical to the surface is received. However, the CCD limits the area in reciprocal space that can be measured within a single image.

We chose the detector-sample distance to be $d = 130$ cm. The Maxipix chip has a side length of 14 mm which results in a resolution of ± 0.34 nm^{-1} in reciprocal space. Thus we focused on the GaAs bragg peak at $Q_{110} = 31.416$ nm^{-1} recording the diffuse intensity at higher Q-values, neglecting the contribution of tensile strained material. Due to the time constraint during the annealing process, a line detector with analyzer crystal could not be applied.

RSM of a [220] reflex were measured before and after annealing. Figure 7 shows a RSM of the [220] GaAs reflection before and after the annealing process. As it can be seen, the diffuse scattering at higher and lower scattering vectors is reduced compared to the state before the annealing process. This implies that the elastic strain, induced by the lattice mismatch of the InAs/GaAs material system has been partially relaxed due to material interdiffusion.[4,18]

A total of 27 RSMs have been measured *in situ* during the annealing process. The sample was annealed for 2 h increasing the temperature to 450 °C stepwise. To monitor the evolution of the strained GaAs substrate during annealing we show cuts through the RSM around the compressed material peak at fixed Q_{110} and Q_{-110} positions respectively for different annealing stages, see Fig. 8. The profiles are shown for the substrate temperatures of 90.3, 90.3, 188.0, 247.1, 292.3, 328.2, 359.8, 360.5, 361.3, and 362.3 °C and annealing times of 4.5, 9.0, 36.0, 49.5, 63.0, 72.0, 81.0, 85.5, 90.0, and 99.0 min.

As it can be seen from the Q_{-110} profile plot, the intensity, originating from the compressively strained GaAs substrate decreases during the temperature ramp. The Q_{110} profile plot indicates that this decrease is accompanied by a shift of the maximum position from $Q_{110} = 31.7$ nm^{-1} to $Q_{110} = 31.6$ nm^{-1} before the maximum is vanishing. This process can be related to strain relaxation due to material interdiffusion.

On the other hand, indium desorption is competing with the diffusion process. This leads to strain relaxation by gallium atoms substituting the desorbed indium atoms. As a result, the indium-content of the QD decreases.[19] However, this process is known to start at higher temperatures than the temperatures applied during our annealing process.[20] Thus, we assume that, the evolution of the scattered diffuse intensity is largely caused the diffusion processes between the QDs and the surrounding media.

V. SUMMARY AND CONCLUSIONS

In this paper we present a new portable MBE system for *in situ* x-ray studies of III/V nanostructures. The system is suitable for investigations at various synchrotron beamlines. The system's main features were described and possible x-ray measurement methods such as GID and GISAXS were found to be compatible to the geometrical constraints imposed by the beryllium windows.

The introduced geometries were tested and first results obtained from *in situ* XRD investigations of the annealing process of InAs QDs were shown. The results indicate that the evolution of the strain field induced by the QDs in the substrate can be successfully investigated during the annealing process.

We believe that the combination of a portable MBE system with a synchrotron light source of high flux and brilliance will help understanding dynamical processes during the growth and post-growth processing of nanostructures, and offering access to large variety of x-ray investigation methods at differently specialized synchrotron beamlines.

ACKNOWLEDGMENTS

Authors would like to thank BMBF for financial support. The *in situ* experiments were performed on the ID03 beamline at the European Synchrotron Radiation Facility (ESRF), Grenoble, France. We are grateful to R. Felici and T. Dufrane at ESRF for providing assistance in using the beamline and dedicated support during the experiments. We also thank to the company "Createc" for implementation of the MBE system design.

[1] J. R. Arthur, Surf. Sci. **500**, 189 (2002).
[2] P. B. Joyce, T. J. Krzyzewski, G. R. Bell, T. S. Jones, S. Malik, D. Childs, and R. Murray, Phys. Rev. B **62**, 10891 (2000).
[3] M. Riotte, E. Fohtung, D. Grigoriev, A. A. Minkevich, T. Slobodskyy, M. Schmidbauer, T. H. Metzger, D. Z. Hu, D. M. Schaadt, and T. Baumbach, Appl. Phys. Lett. **96**, 083102 (2010).
[4] D. Hu, A. Trampert, and D. Schaadt, J. Cryst. Growth **312**, 447 (2010).
[5] T. H. Metzger, T. U. Schlli, and M. Schmidbauer, C. R. Phys. **6**, 47 (2005).
[6] D. Fong, C. Lucas, M. Richard, and M. Toney, MRS Bull. **35**, 504 (2010).
[7] M. Albrecht, H. Antesberger, W. Moritz, H. Plockl, M. Sieber, and D. Wolf, Rev. Sci. Instrum. **70**, 3239 (1999).
[8] A. Barbier, O. Robach, O. Ulrich, A. Mougin, G. Brard, R. Baudoing-Savois, M. De Santis, M. C. Saint-Lager, P. Dolle, O. Geaymond, P. Taunier, P. Jeantet, J. P. Roux, and G. Renaud, Nucl. Instrum. Methods Phys. Res. B **149**, 213 (1999).
[9] P. Bernard, K. Peters, J. Alvarez, and S. Ferrer, Rev. Sci. Instrum. **70**, 1478 (1999).
[10] S. Couet, T. Diederich, K. Schlage, and R. Rohlsberger, Rev. Sci. Instrum. **79**, 093908 (2008).
[11] P. Fuoss and I. Robinson, Nucl. Instrum. Methods Phys. Res. **222**, 171 (1984).
[12] B. Jenichen, W. Braun, V. M. Kaganer, A. G. Shtukenberg, L. Daweritz, C. Schulz, K. H. Ploog, and A. Erko, Rev. Sci. Instrum. **74**, 1267 (2003).
[13] S. Stankov, R. Ruffer, M. Sladecek, M. Rennhofer, B. Sepiol, G. Vogl, N. Spiridis, T. Slezak, and J. Korecki, Rev. Sci. Instrum. **79**, 045108 (2008).
[14] H. Tajiri, K. Sumitani, S. Nakatani, T. Takahashi, K. Akimoto, H. Sugiyama, X. Zhang, and H. Kawata, Appl. Surf. Sci. **237**, 641 (2004).
[15] E. Vlieg, A. Van't Ent, A. De Jongh, H. Neerings, and J. Van Der Veen, Nucl. Instrum. Methods Phys. Res. A **262**, 522 (1987).
[16] P. M. J. Maree, A. P. De Jongh, J. W. Derks, and J. F. Van Der Veen, Nucl. Instrum. Methods Phys. Res. B **28**, 76 (1987).
[17] T. Schallenberg, L. W. Molenkamp, and G. Karczewski, Phys. Rev. B **70**, 155328 (2004).
[18] Y. Qiu, Z. Y. Zhang, R. A. Hogg, A. G. Cullis, and T. Walther, J. Phys.: Conf. Ser. **209**, 012036 (2010).
[19] A. Jackson, P. Pinsukanjana, L. Coldren, and A. Gossard, J. Cryst. Growth **175**, 244 (1997).
[20] C. Heyn, Phys. Rev. B **66**, 075307 (2002).